

Preparation and optical dispersion and absorption of Ag-photodoped $\text{Ge}_x\text{Sb}_{40-x}\text{S}_{60}$ ($x = 10, 20$ and 30) chalcogenide glass thin films

E Márquez^{1,3}, J M González-Leal¹, A M Bernal-Oliva¹,
T Wagner² and R Jiménez-Garay¹

¹ Departamento de Física de la Materia Condensada, Facultad de Ciencias, Universidad de Cádiz, Campus de Puerto Real, 11510 – Puerto Real, Andalucía, Spain

² Department of General and Inorganic Chemistry, University of Pardubice, 53210 – Pardubice, Czech Republic

E-mail: emilio.marquez@uca.es

Received 16 May 2007, in final form 8 June 2007

Published 16 August 2007

Online at stacks.iop.org/JPhysD/40/5351

Abstract

We have analysed the effect of silver content on the optical properties of Ag-photodoped amorphous $\text{Ge}_x\text{Sb}_{40-x}\text{S}_{60}$ (with $x = 10, 20$ and 30 at.%) chalcogenide thin films; the chalcogenide host layers were prepared by vacuum thermal evaporation. Films of composition $\text{Ag}_y(\text{Ge}_x\text{Sb}_{40-x}\text{S}_{60})_{100-y}$, with $y \lesssim 10$ at.%, were prepared by successively photodissolving about 10 nm thick layers of silver. The film thickness and optical constants have been accurately determined by a refined envelope method, based upon the two envelope curves of the optical-transmission spectrum, obtained at normal incidence. The dispersion of the linear refractive index of the Ag-photodoped chalcogenide films is analysed in terms of the Wemple–DiDomenico single-effective-oscillator model. We have found that the maximum change in the index of refraction, between the Ag-photodoped and the undoped material, is about 0.08, when the Ag-concentration reaches the level of saturation of around 10 at.%. On the other hand, the Tauc gap, E_g^{opt} , decreases notably, with increasing Ag-content: for instance, in the particular case of $x = 10$ at.%, the smallest Ge-content, E_g^{opt} decreases from 1.97 down to 1.67 eV.

1. Introduction

Chalcogenide glasses, based on S, Se and Te, have many unique optical properties, which can be used for a wide variety of applications [1]. These glasses are very promising materials for use in optical elements, such as gratings [2], optical recording media [3] and in fibre optics and guided-wave devices in integrated optics, since they certainly exhibit good transparency in the infrared region, especially at the telecommunication wavelengths, 1.3 and 1.55 μm [4]. Moreover, the chalcogenide glasses possess a high third-order

nonlinearity, with an ultrafast time response [1, 5]. The nonlinear refractive index, n_2 , of Ag-doped chalcogenide glasses is generally higher than that of the undoped glasses, because the Ag-doped chalcogenides have higher linear refractive index, n —the presence of silver (transition-metal) atoms, with easily polarizable electron clouds, is a clear advantage for the effect. It should be pointed out that, recently, Ogusu *et al* [6] developed $\text{Ag}_y(\text{As}_{0.4}\text{Se}_{0.6})_{100-y}$ glasses, with n_2 greater than 2000 times that of fused silica, by the corresponding addition of Ag into As_2Se_3 glasses.

Optically-induced dissolution and diffusion of some metals (Ag, Cu, Zn, and Cd), in amorphous chalcogenides, has

³ Author to whom any correspondence should be addressed.

been extensively investigated by many authors [7–12] and has not been fully explained as yet. Understanding the kinetics of the photodoping process, and finding new, suitable host glass-matrices, is, indeed, a crucial point for all technological applications. In addition, the technique of the photodissolution of Ag, step-by-step and at room temperature, into amorphous chalcogenide films, allows the preparation of homogeneous films with exactly the desired silver concentration and thickness [13]. The amorphous ternary films with chemical composition $\text{Ge}_x\text{Sb}_{40-x}\text{S}_{60}$ are appropriate, in combination with Ag-photodoping, because layers of good optical quality, with a reasonably broad range of silver-content, could be obtained; in a previous paper [14], we have reported in detail on the optical dispersion and absorption and also on the structure of the corresponding undoped Ge–Sb–S chalcogenide glassy samples. So, the aim of the present work was, firstly, to prepare these Ag-doped $\text{Ge}_x\text{Sb}_{40-x}\text{S}_{60}$ (with $x = 10, 20$ and 30 at.%) chalcogenide films and, secondly, to study their respective linear optical properties—we believe that this is the first time that a systematic optical characterization of such glassy alloy films is presented.

2. Experimental procedures

The chalcogenide host thin films were synthesized using the well-established vacuum thermal evaporation technique. To produce the bulk glass for the evaporation source, the constituents were measured into a quartz tube, vacuum-sealed and melted in a rocking furnace for 24 h at 1000°C and, subsequently, quenched in air. Fragments of the bulk material were used to evaporate the films in a vacuum chamber with a residual pressure of approximately 1×10^{-4} Pa and at a rate of around 1 nm s^{-1} ; the deposition rate was continuously measured by the dynamical weighing procedure.

X-ray diffraction measurements showed that all the films to be studied were amorphous, and their chemical compositions were checked by EDX-analysis. The thicknesses of the films ranged between about 700 and 1200 nm, which are appropriate for the accurate evaluation of all the optical parameters, considering the total number of interference fringes existing in the optical-transmission spectra, by the refined envelope method used in the present work, previously reported in detail by Gonzalez-Leal *et al* [15]. It should be emphasized that we have not found any appreciable influence of the film thickness on the optical properties of the starting undoped Ge–Sb–S samples, in the 700–1200 nm range.

Next, different layers of silver were evaporated on top of the chalcogenide host. For the Ag-deposition we used an Al_2O_3 -covered tungsten boat, thereby reducing notably both the heat and light exposure of the samples, during the evaporation process. Photodoping was carried out by illuminating the samples with a 500 W tungsten lamp, equipped with a large Fresnel lens and an IR cut-off filter. During the light exposure, the samples were carefully sandwiched between two other glass plates, in order to avoid surface oxidation. The Ag-concentration of our Ag-photodoped samples ranged between around 1 and 10 at.% (it reached the level of saturation). When preparing layers with a relatively large Ag-content, we always found that photodissolving a relatively thick layer of silver, in

just one step, resulted in a photodoped product that was rather inhomogeneous. However, doping the chalcogenide host, step-by-step, by consecutively dissolving ~ 10 nm thick layers of silver, produced a homogeneous sample, without silver remaining on top of this sample, after completing the illumination. The values of the silver concentration quoted were determined from the measurements of the silver and the chalcogenide layer thicknesses.

The room-temperature optical-transmission spectra, at normal incidence, of the samples, were recorded over the 300 up to 2500 nm spectral region, by a double-beam UV/Vis/NIR spectrophotometer (Perkin-Elmer, model Lambda-19). The area of illumination over which the transmission spectra were obtained is $1 \text{ mm} \times 10 \text{ mm}$. It should be pointed out that the transmission spectra of the doped thin-film samples were those corresponding to weakly-absorbing thin layers, with uniform thickness—the absence of shrinkage in the amplitude of the interference fringes of those transmission spectra is clear evidence of the thickness uniformity of the Ag-photodoped films [16]. Finally, the thicknesses of the films were also directly measured by a stylus-based surface profiler (Sloan, model Dektak IIA), with an accuracy of ± 5 nm, in order to systematically cross-check the results derived from the application of the optical-characterization method with the optical-transmission spectra.

3. Results

The transmission spectra of two representative undoped and Ag-photodoped amorphous $\text{Ge}_x\text{Sb}_{40-x}\text{S}_{60}$ thin-film samples are plotted in figure 1. Judging from these experimental

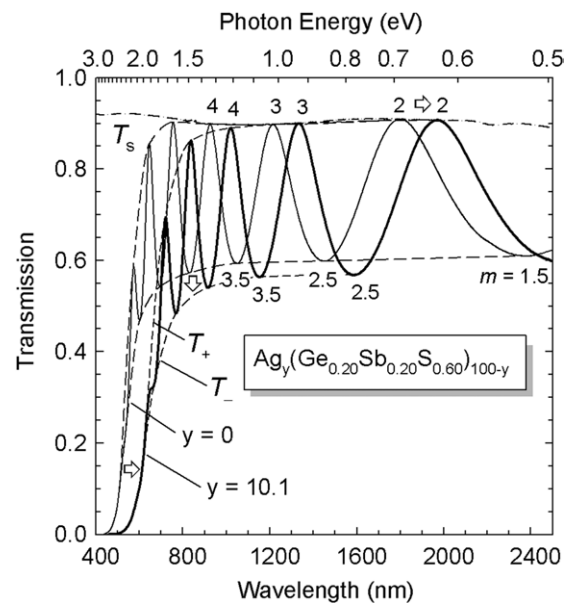


Figure 1. Room-temperature optical-transmission spectra (at normal incidence), of two representative undoped and Ag-photodoped amorphous $\text{Ge}_{20}\text{Sb}_{20}\text{S}_{60}$ thin films, deposited onto slightly-absorbing, 1 mm thick, borosilicate glass substrates (Menzel–Gläser microscope slides). The transmission spectrum of the bare substrate, T_s , is also conveniently plotted in the graph. The top and bottom envelope curves, T_+ and T_- , have been computer drawn using the algorithm developed by McClain *et al* [17].

Table 1. Thicknesses corresponding to the different undoped and Ag-photodoped (fully saturated) amorphous $\text{Ge}_x\text{Sb}_{40-x}\text{S}_{60}$ chalcogenide films. Also, the number of ‘Ag-photodoping steps’, their respective thicknesses and the values of the accumulated total Ag-thickness, the final Ag-concentration and the sample thickness contraction.

Ge-content (at. %)	Undoped sample thickness, $d_{\text{Ge-Sb-S}}^{\text{initial}}$ (nm)	Number of Ag layers (thicknesses of Ag layers (nm))	Accumulated silver thickness, $d_{\text{Ag}}^{\text{accumulated}}$ (nm)	Maximum Ag-content (at.%)	$d_{\text{Ge-Sb-S}}^{\text{initial}}$ + $d_{\text{Ag}}^{\text{accumulated}}$ (nm)	Photodoped sample thickness, $d_{\text{Ge-Sb-S}}^{\text{final}}$ (nm)	Thickness contraction (%)
10	1195 ± 6 (0.5%)	6 (10,8,12,10,10 and 10)	60	7.6	1255	1233 ± 7 (0.6%)	1.7
20	710 ± 5 (0.7%)	5 (10,8,12,10 and 10)	50	10.1	760	751 ± 7 (0.9%)	1.2
30	950 ± 5 (0.5%)	5 (10,8,12,10 and 10)	50	7.7	1000	996 ± 9 (0.9%)	0.4

results, a clear red-shift occurs in the interference-free region of the spectra, with increasing Ag-content. Such a shift, as discussed later in the paper, is a consequence of the decrease of the corresponding optical band gap, when the Ag-content is increased. Also, an increase in the amplitude of the optical-interference fringes, resulting from Ag-photodoping, can be seen in figure 1: this unambiguously reflects an increase in the linear refractive index of the photodoped sample.

The values of the thickness, d , linear refractive index, n , and absorption coefficient, α , of all the films being studied, have been determined only from their normal-incidence transmission spectra, using the previously mentioned envelope method that, significantly, takes into account the slight absorption existing in the glass substrate and whose wavelength-dependent refractive index is about 1.5. Thus, film-thickness values, and, correspondingly, refractive-index values, with accuracies better or around 1%, have always been achieved—see table 1 in [15], where more detailed information about the accuracy of the thin-film thicknesses can be found. The d -values and their respective uncertainties, calculated by the envelope method, are all listed in table 1. Alternatively, these values of the thickness were, as indicated above, directly measured by the mechanical profilometer, and the differences found between the mechanically-measured and optically-calculated values were, in all cases, less than 3%. In addition, it is necessary to stress that there is no loss in transmission in the long-wavelength region of the spectra, as is the case in other chalcogenide films [14] (see figure 1); in other words, in the transparent region, the top envelopes of the two transmission spectra, T_+ , practically coincide with the transmission spectrum of the bare substrate, and it is, certainly, the direct result of the absence of any optically-detectable surface roughness in the samples subjected to study.

Returning to table 1, it should be noted that the Ag-photodoped-film-thickness values show that the final sample thickness, once the highest Ag-concentration has been reached, $d_{\text{Ag-Ge-Sb-S}}^{\text{final}}$, is slightly smaller, or practically equal, to the sum of the undoped sample thickness, i.e. the initial thickness, $d_{\text{Ge-Sb-S}}^{\text{initial}}$, and the accumulated total Ag-thickness, $d_{\text{Ag}}^{\text{accumulated}}$. $d_{\text{Ag-Ge-Sb-S}}^{\text{final}} \lesssim d_{\text{Ge-Sb-S}}^{\text{initial}} + d_{\text{Ag}}^{\text{accumulated}}$. So, in the case, for example, of the composition with the smallest Ge-content, $\text{Ge}_{10}\text{Sb}_{30}\text{S}_{60}$, the thickness changed from 1195 ± 6 nm, for the undoped film, up to 1233 ± 7 nm, after photodissolving a total amount of Ag of 60 nm, with six ‘Ag-photodoping steps’ of thicknesses 10 nm, 8 nm, 12 nm, 10 nm, 10 nm and 10 nm, respectively. The difference between the value of the sum of thicknesses, $d_{\text{Ge-Sb-S}}^{\text{initial}} + d_{\text{Ag}}^{\text{accumulated}}$, 1255 nm, and the value of $d_{\text{Ag-Ge-Sb-S}}^{\text{final}}$, was, therefore, 22 nm, which means a

relative thickness contraction of 1.7%. A decrease of the Ag-photodoped-product thickness has also been reported by Kawaguchi and Masui [18], in the cases of the close binary chalcogenide compositions $\text{Ge}_{30}\text{S}_{70}$ and $\text{As}_{40}\text{S}_{60}$. Moreover, as seen in table 1, the observed sample thickness contraction decreases with increasing Ge-content. This could be related to the accompanying increase in the number of $\text{GeS}_{4/2}$ tetrahedral structural units, which are increasingly present in the atomic structure of the Ge–Sb–S samples [14], as the Ge-content increases.

On the other hand, the optical-characterization method proposed by González-Leal *et al* [15] provided values of the index of refraction, at the particular wavelengths, λ_{tan} , where the transmission spectra are tangential to their top and bottom envelope curves, T_+ and T_- [16]. It is worth recalling at this point the basic equation for the appearance of optical-interference fringes, $2n(\lambda_{\text{tan}})d = m\lambda_{\text{tan}}$, where m is the order number, see figure 1, in which some m -values are introduced for illustrative purposes. Additionally, the spectral dependence (dispersion) of the refractive index, in the visible and near-infrared regions, was analysed in terms of the Wemple–DiDomenico (WDD) single-effective-oscillator model [19, 20], whose mathematical expression is the following:

$$\varepsilon_1(\omega) = n^2(\omega) = 1 + \frac{E_o E_d}{E_o^2 - (\hbar\omega)^2}, \quad (1)$$

where $\hbar\omega$ is the photon energy, E_o is the oscillator energy and E_d is the so-called dispersion energy. Plots of the refractive-index factor $(n^2 - 1)^{-1}$ versus $(\hbar\omega)^2$, for some representative Ag–Ge–Sb–S alloy films being studied, are shown in figure 2, along with their corresponding least-squares straight lines; the Ag-content dependence of the static refractive index, n ($\hbar\omega = 0$), is also displayed, as an inset, in figure 2. It is to be emphasized the goodness of the linear fits to the larger-wavelength data. The typical behaviour of the dispersion of n is observed in all the cases: the experimental frequency variation in the refractive index clearly departs from that given by equation (1), when the photon energy approaches the optical band gap, E_g^{opt} (interband absorption). The dependences of the WDD dispersion parameters, E_o and E_d , on the Ag-content, for all the samples subjected to study, are shown in figures 3(a) and (b).

Once the values of the refractive index are known in the working spectral region, in terms of equation (1), the optical-absorption spectra of the present chalcogenide alloy films were then derived from the upper envelope, T_+ , of their transmission spectra [15]. Some of the calculated spectra of

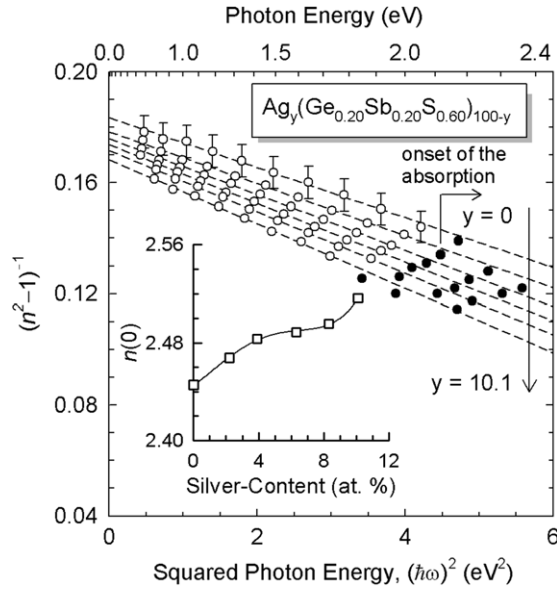


Figure 2. WDD fits of the optical-dispersion data corresponding to undoped and Ag-photodoped $\text{Ge}_{20}\text{Sb}_{20}\text{S}_{60}$ thin-film samples. The dashed straight lines are linear least-squares fits. In the inset, the variation of the static refractive index, $n(\hbar\omega = 0)$, with the Ag-content, for these particular samples; the solid line is to guide the eye.

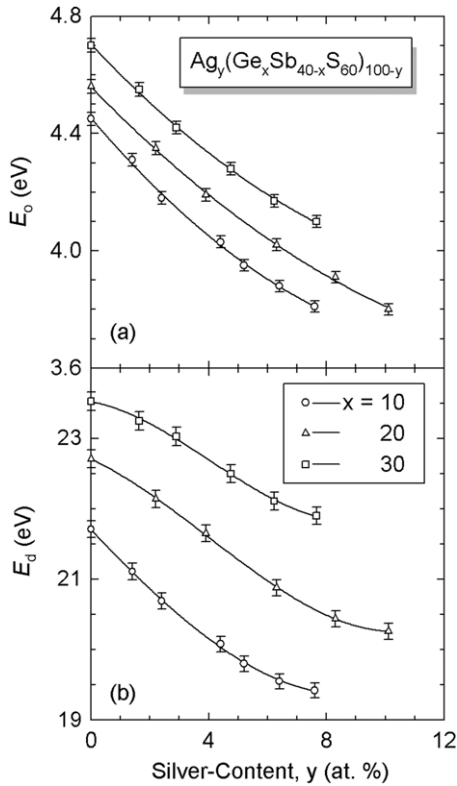


Figure 3. Compositional dependences of the single-effective-oscillator parameters E_o and E_d . All the solid lines are to guide the eye.

α are displayed in figure 4(a), using a logarithmic scale: in order to complete the computation of the optical constants (n, k), the dimensionless extinction coefficient, k , is easily obtained from the already-known α -values, using the basic

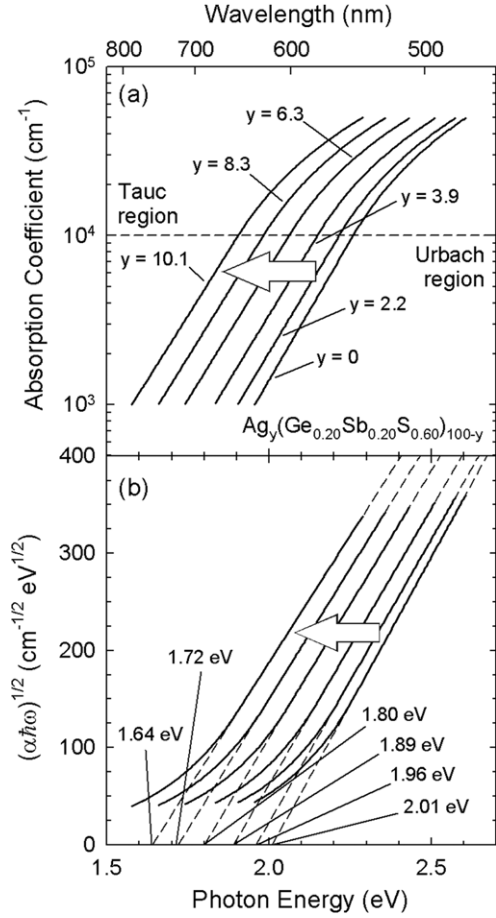


Figure 4. (a) Optical-absorption spectra of the undoped and Ag-photodoped amorphous $\text{Ge}_{20}\text{Sb}_{20}\text{S}_{60}$ films. (b) Determination of the optical band gaps, in terms of Tauc's law, as linear extrapolation (dashed straight lines) of the high-energy (or, equivalently, high-absorption) data.

formula, $k = \alpha\lambda/4\pi$. Next, the optical gap, E_g^{opt} , was determined, according to the generally accepted 'non-direct transition' model for amorphous semiconductors, proposed by Tauc [21], from the intercept on the energy-axis of the linear fit of the larger-energy data, in a plot of $(\alpha\hbar\omega)^{1/2}$ versus $\hbar\omega$ —the corresponding Tauc plots are shown in figure 4(b). This implies the following equation:

$$(\alpha\hbar\omega)^{1/2} = B^{1/2}(\hbar\omega - E_g^{\text{opt}}), \quad (2)$$

where $B^{1/2}$ is the so-called Tauc slope. This relationship assumes that the densities of the electron states in the valence and conduction bands, near the band gap, have a parabolic distribution and, also, that the matrix elements for the interband transitions associated with the photon absorption are equal for all the transitions.

4. Discussion

The Wemple–DiDomenico single-oscillator parametrization of the optical-dispersion curves [19] was the first approach that attached physical significance to the dispersion parameters. Relating the Kramers–Kronig equation for the real part of the

dielectric function:

$$\varepsilon_1(\omega) - 1 = \frac{2}{\pi} \text{P} \int_0^{\infty} \frac{\omega' \varepsilon_2(\omega')}{\omega'^2 - \omega^2} d\omega', \quad (3)$$

to equation (1), we can have an insight into this proposed physical meaning. So we can write

$$\frac{E_o E_d}{E_o^2 - (\hbar\omega)^2} = \frac{2}{\pi} \text{P} \int_0^{\infty} \frac{\omega' \varepsilon_2(\omega')}{\omega'^2 - \omega^2} d\omega'. \quad (4)$$

Next, by expanding both sides of equation (4), in powers of ω^2 , and equating the coefficients of the different terms, we finally obtain:

$$E_o^2 = \frac{M_{-1}}{M_{-3}} \quad (5)$$

and

$$E_d^2 = \frac{M_{-1}^3}{M_{-3}}, \quad (6)$$

where we have introduced the r th moment of the optical spectrum, which is defined as follows:

$$M_r = \frac{2}{\pi} \int_0^{\infty} E^r \varepsilon_2(E) dE. \quad (7)$$

As we can see from equation (5), E_o does not depend on the scale of $\varepsilon_2(E)$, because the numerator and the denominator are of the same power; thus, the oscillator energy, E_o , is considered an *average* band gap, the so-called WDD gap, and it corresponds to the distance between the ‘centres of gravity’ of the valence and the conduction bands: E_o is, therefore, related to the bond energy of the different chemical bonds present in the material. In this way, the strong decrease observed in the dispersion parameter, E_o , with increasing Ag-content (see figure 3(a)), for the Ag–Ge–Sb–S films under study, is mainly due to the lower bond energy of Ag–S bonds, 217 kJ mol⁻¹ [22], in comparison with those corresponding to Ge–S and S–S bonds, 551 kJ mol⁻¹ and 425 kJ mol⁻¹, respectively.

On the other hand, unlike E_o , the dispersion energy, E_d , does depend upon the scale of $\varepsilon_2(E)$, and, as a result, serves as a measure of the strength of the interband transitions. An important achievement of the WDD model is that it relates the dispersion energy to other physical parameters of the material, through a simple empirical formula [19, 20]:

$$E_d = \beta N_c Z_a N_e \quad (\text{eV}), \quad (8)$$

where β is a two-valued parameter, with an ‘ionic’ or ‘covalent’ value ($\beta_i = 0.26 \pm 0.03$ eV and $\beta_c = 0.37 \pm 0.04$ eV, respectively), N_c is the coordination of the cation nearest neighbour to the anion, Z_a is the formal chemical valency of the anion and N_e is the total number of valence electrons, cores excluded, per anion.

The incorporation of Ag into the structure of the present Ge_xSb_{40-x}S₆₀ glass films has the effect of decreasing the WDD dispersion parameter E_d (see figure 3(b)). Hence, as an appropriate approximation [23], the addition of silver into the ternary chalcogenide matrix decreases one or other of the

quantities on the right-hand side of equation (8). Even if Ag-photodoping were to change the nature of the chemical bonding towards being less ionic, considering the electronegativities of the different types of atoms present in the material, this, undoubtedly, cannot be the major factor, since this particular factor would increase the parameter β ($\beta_c > \beta_i$). Furthermore, in less ionic materials, the smaller s–p splitting increases the parameter N_e , which is, again, against the observed trend in the dispersion energy. For this reason, in our case of Ag_y(Ge_xSb_{40-x}S₆₀)_{100-y} thin-film samples, it is reasonable to assume that the average cation coordination is the factor that is most affected by the addition of Ag to the glassy structure; it must also be taken into account that $Z_a = 2$ remains valid for all the samples.

On the other hand, it is to be mentioned that there is a substantial difference between the Ag-photodoping process of As₂S₃ (reference composition) glass films, compared with that in GeS₂ and GeSe₂ glass films. The photodoping of GeS₂ with Ag, at concentrations of 16 at.%, results in the destruction of $6 \pm 3.5\%$ of GeS_{4/2} tetrahedral structural units, whereas in the GeSe₂ layers photodoped up to 20 at.% by silver, $12 \pm 3.5\%$ of the initial number of the GeSe_{4/2} tetrahedra are destroyed [24]. The demolishing of structural units in the Ge-based chalcogenide glasses, with Ag-photodoping, and their conservation in the arsenic sulfide glass, which is formed, mainly, by eventually well-preserved pyramidal As₂S_{3/2} molecules, are obviously conditioned by the more rigid structures of GeS₂ and GeSe₂ amorphous networks. Moreover, although the introduction of Sb, forming, mainly, SbS_{3/2} pyramidal structural units, appears to ‘soften’ the otherwise rigid Ge–S network [25], it seems plausible to finally propose that photodoping with Ag the present ternary alloys will decrease their effective cation coordination number, N_c , as a consequence of the destruction of certain structural units, and, therefore, according to equation (8), the dispersion energy, E_d , will also decrease, as has been empirically found.

In the compositional dependence of the static refractive index, $n(0)$ ($=\sqrt{1 + E_d/E_o}$), shown in the inset of figure 2, and corresponding to the representative case of Ag_y(Ge_{0.20}Sb_{0.20}S_{0.60})_{100-y} sample, a relatively moderate increase, with increasing Ag-content, can be seen, which is straightforwardly explained, according to the Lorentz–Lorenz equation, by the larger electronic polarizability of the transition-metal atoms of Ag, with more easily polarizable electron clouds and having a covalent radius of 153 pm [26], in comparison with the electronic polarizabilities of Ge, Sb and S atoms, with smaller covalent radii of 122 pm, 138 pm and 102 pm, respectively. Also, the origin of the plateau, evident in the inset of figure 2, between around 4 and 8 at.% of silver, is not certain, but it may well arise from a fundamental change in the structure of the Ag-photodoped film, over this particular compositional range. In addition, a clear red-shift of the optical-absorption edge is observed in figure 4(a), with increasing Ag-content, again for the representative sample of composition Ag_y(Ge_{0.20}Sb_{0.20}S_{0.60})_{100-y}. It should be stressed that following the Kramers–Kronig relationship for the real part of the dielectric function, equation (3), the red-shift in the optical-absorption spectrum must necessarily give an increased refractive index, as experimentally obtained. It is worth expressing here the fundamental relationship, equivalent

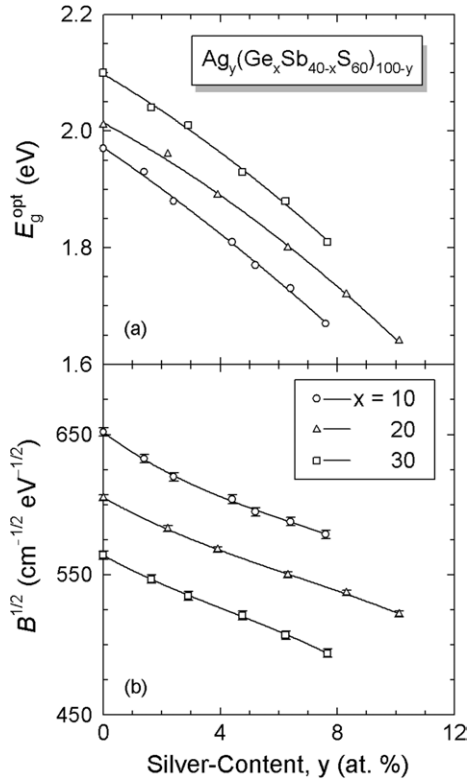


Figure 5. Tauc gap (a) and slope (b), versus Ag-content, for each of the chalcogenide compositions under investigation. All the solid lines are to guide the eye.

to equation (3), which is derived by setting $\omega = 0$: $n(0) - 1 = (1/2\pi^2) \int_0^\infty \alpha(\lambda) d\lambda$, which allows checking the consistency of the values of the static refractive index and the relative positions of the optical-absorption edges. That is, it should be verified that the higher the value of $n(0)$, the larger the area under the absorption curve.

Continuing with the analysis of the different physical quantities, as can be noted in figure 5, the Tauc gap decreases notably with the Ag-content, for all the compositions studied. For instance, in the particular case of a Ge-content of 10 at.%, E_g^{opt} decreases from 1.97 down to 1.67 eV, when the Ag-concentration in the sample increases from zero up to the maximum value corresponding to the smallest Ge-content, 7.6 at.%. This fact could be explained if we consider that, as the silver is photodoped, it, acting as a cation, joins mainly S atoms: the incorporation of silver into the structure of the Ge-Sb-S alloys is expected to produce preferentially the breaking of S-S homopolar bonds, belonging to S_8 -rings or S-ring fragments, and Ge-S heteropolar bonds, belonging to edge-sharing-type $\text{GeS}_{4/2}$ structural units [12]. Interestingly, the existing pyramidal $\text{SbS}_{3/2}$ structural units presumably will *not* be destroyed, as the Ag is photodissolved. If we now take again into consideration the bond energies of the S-S and Ge-S bonds (425 kJ mol^{-1} and 551 kJ mol^{-1} , respectively) and that of the Ag-S bonds (217 kJ mol^{-1}), the Ag-photodoping is obviously expected to give place to a remarkable decrease in the Tauc gap, as experimentally found.

Next, we examine the empirical correlation between the WDD and the Tauc gaps (see figure 6). As seen in this graph of E_o versus E_g^{opt} , for the Ag-Ge-Sb-S films, it is

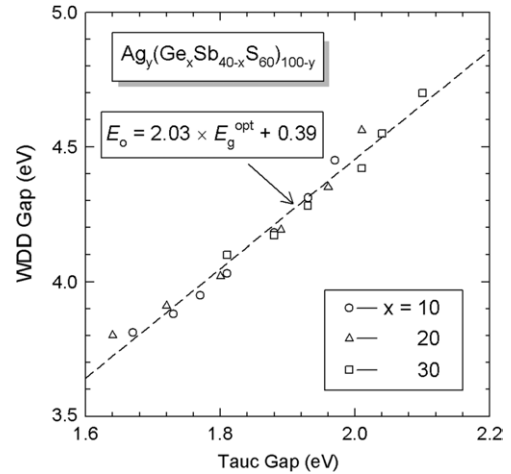


Figure 6. The relationship between the parameter E_o and E_g^{opt} , for the Ag-Ge-Sb-S thin-film samples. The dashed straight line is a linear least-squares fit (the corresponding correlation coefficient is 0.987).

verified that $E_o = 2.03 \times E_g^{\text{opt}} + 0.39$. According to Tanaka [27], the correspondence between the parameters E_o and E_g^{opt} , in the case of amorphous chalcogenides, is expressed functionally as $E_o \approx 1.9 \times E_g^{\text{opt}}$; also, more recently, Ticha and Tichy [28] have found the following phenomenological relation, for the two gaps under consideration: $E_o = 1.25 \times E_g^{\text{opt}} + 1.50$. These two previously reported relationships were obtained from considering values of E_o and E_g^{opt} corresponding to binary compositions, whereas in the present case, the data, significantly, belong to much more complex, from the point of view of the electron band structure, quaternary chalcogenide alloys. Finally, the B -factor, in equation (2), is inversely related to the product of the already calculated static refractive index, $n(0)$, and the localized-state tail width, ΔE_{tail} [29–31], and it is, therefore, a clear indicator of the degree of randomness of the atomic structure of amorphous semiconductors. So, from the values of the Tauc slope, $B^{1/2}$, shown in figure 5(b), it is concluded that the silver incorporation in Ge-Sb-S chalcogenide films tends to increase monotonically the degree of disorder of the glassy structure; it must be mentioned that the decrease found in the values of the parameter B is much more pronounced than the increase observed in the values of the static refractive index, and, thus, the parameter $\Delta E_{\text{tail}} (\propto [n(0)B]^{-1})$, as inferred from above), increases with the incorporation of silver.

5. Concluding remarks

Silver-doped amorphous $\text{Ge}_x\text{Sb}_{40-x}\text{S}_{60}$ (with $x = 10, 20$ and 30 at.%) thin films have been prepared by the room-temperature step-by-step photodoping technique; the chalcogenide host layers were deposited by vacuum thermal evaporation. The film thickness and optical constants have been accurately determined by a refined envelope method, based upon the two envelope curves of the optical-transmission spectrum, obtained at normal incidence. We have analysed in detail the optical-dispersion data, using the WDD single-effective-oscillator model. Photodissolution of Ag into the ternary chalcogenide matrix introduces new

Ag–S bonds, which explains the substantial decrease in the WDD and Tauc gaps, with the Ag-content. On the other hand, we attribute the observed decrease in the dispersion energy, with increasing Ag-content, mainly to the decrease in the overall, effective cation coordination number. Lastly, the maximum change in the linear refractive index found in the present work, between the Ag-photodoped and the undoped material, about 0.08, when the Ag-concentration reaches the level of saturation of around 10 at.%, makes these Ge–Sb–S chalcogenide glass films potential candidates as optical recording media.

Acknowledgments

This work has been supported by the MICYT (Spain) and the FEDER (EU), under FIS2005-01409 research project.

References

- [1] Zakery A and Elliott S R 2003 *J. Non-Cryst. Solids* **330** 1
- [2] González-Leal J M, Krecmer P, Prokop J and Elliott S R 2003 *J. Non-Cryst. Solids* **326–327** 416
- [3] Ohta T 2001 *J. Optoelectron. Adv. Mater.* **3** 609
- [4] Sanghera J S and Aggarwal I D 1999 *J. Non-Cryst. Solids* **256–257** 6
- [5] Harbold J M, Ilday F Ö, Wise F W, Sanghera J S, Nguyen V Q, Shaw L B and Aggarwal I D 2002 *Opt. Lett.* **27** 119
- [6] Ogusu K, Yamasaki J, Maeda S, Kitao M and Minakata M 2004 *Opt. Lett.* **29** 265
- [7] Kostyshin M T, Mikhailovskaya E V and Romanenko P F 1966 *Sov. Phys.—Solid State* **8** 451
- [8] Kolobov A V and Elliott S R 1991 *Adv. Phys.* **40** 625
- [9] Márquez E, Jiménez-Garay R, Zakery A, Ewen P J S and Owen A E 1991 *Philos. Mag. B* **63** 1169
- [10] Wagner T, Márquez E, Fernández-Peña J, González-Leal J M, Ewen P J S and Kasap S O 1999 *Philos. Mag. B* **79** 223
- [11] Márquez E, Wagner T, González-Leal J M, Bernal-Oliva A M, Prieto-Alcón R, Jiménez-Garay R and Ewen P J S 2000 *J. Non-Cryst. Solids* **274** 62
- [12] Wagner T and Frumar M 2003 *Photo-induced Metastability in Amorphous Semiconductors* ed A V Kolobov (Weinheim: Wiley-VCH) p 160
- [13] Wagner T, Munzar M, Krbal M and Kasap S O 2005 *Thermochim. Acta* **432** 241
- [14] Márquez, Bernal-Oliva A M, González-Leal J M, Prieto-Alcón R and Wagner T 2006 *J. Phys. D: Appl. Phys.* **39** 1793
- [15] González-Leal J M, Prieto-Alcón R, Angel J A, Minkov D A and Márquez E 2002 *Appl. Opt.* **41** 7300
- [16] Swanepoel R 1984 *J. Phys. E: Sci. Instrum.* **17** 896
- [17] McClain M, Feldman A, Kahaner D and Ying X 1991 *Comput. Phys.* **5** 45
- [18] Kawaguchi T and Masui K 1987 *Japan. J. Appl. Phys.* **26** 15
- [19] Wemple S H and DiDomenico Jr. M 1971 *Phys. Rev. B* **3** 1338
- [20] Wemple S H 1973 *Phys. Rev. B* **7** 3767
- [21] Tauc J 1974 *Amorphous and Liquid Semiconductors* ed J Tauc (New York: Plenum) p 159
- [22] Kerr J 1996 *Chemical Rubber Company Handbook of Chemistry and Physics* 77th edn ed D R Lide (Boca Raton, FL: CRC)
- [23] González-Leal J M, Angel J A, Krecmer P, Márquez E and Jiménez-Garay R 2006 *Phys. Rev. B* **74** 205204
- [24] Stetsun A T, Indutnyi I Z and Kravets V G 1996 *J. Non-Cryst. Solids* **202** 113
- [25] Kotsalas I P, Papadimitriou D, Raptis C, Vlcek M and Frumar M 1998 *J. Non-Cryst. Solids* **226** 85
- [26] <http://www.webelements.com>
- [27] Tanaka Ke 1980 *Thin Solid Films* **66** 271
- [28] Tichá H and Tichý L 2002 *J. Optoelectron. Adv. Mater.* **4** 381
- [29] Mott N F and Davis E A 1979 *Electronic Processes in Non-Crystalline Materials* 2nd edn (Oxford: Clarendon)
- [30] Zanatta A R and Chambouleyron I 1996 *Phys. Rev. B* **53** 3833
- [31] Tichý L, Tichá H, Nagels P and Callaerts R 1998 *Mater. Lett.* **36** 294